Biomass Conversion and Biorefinery
https://doi.org/10.1007/s13399-023-03950-2

ORIGINAL ARTICLE

Eco-friend shellfish powder of the mussel *Brachidontes variabilis* for uptake lead (II) ions

Safaa A. Mahmoud[1] · Adel S. Orabi[2] · Lamiaa I. Mohamedein[3] · Khalid M. El-Moselhy[3] · Eman M. Saad[1]

Received: 10 November 2022 / Revised: 29 January 2023 / Accepted: 14 February 2023

Abstract
This study aims to employ clam powder as an environmentally acceptable sorbent to capture lead(II) from an aquatic media. Mussel *Brachidontes variabilis* "*Mytilus arabicus*" shells collected from the intertidal zone of the Gulf of Suez for producing shellfish powder (SFP). Before and after lead loading, SFP sorbent was characterized using X-ray fluorescence (XRF), Fourier transform infrared (FT-IR) spectra, transmission electron microscope (TEM), scanning electron microscope (SEM) equipped with energy dispersive X-ray (EDS), and X-ray diffraction (XRD). Maximum Pb(II) ion removal capacity of SFP sorbent was done as a function of shacking duration interval, SFP particle size, pH, Pb (II) ion concentration, SFP dose, temperature, and agitation rate. Numerous mathematical kinetic and isothermal approaches were used to equilibrium experimental data to validate the highest bio-sorption capabilities of SFP (in mg g^{-1}). Optimal conditions were determined to be 90 min, 0.063 mm SFP particle size, pH 5.5, 130 mg L^{-1} Pb(II) ions in 50 mL solution, 0.05 g SFP, 25^{o} C, and 250 rpm. In this sorption process, the Qasi-1st order and monolayer Langmuir isothermal simulations were prominent. In terms of thermodynamics, the capturing of Pb (II) by SFP was spontaneous ($-\Delta G^o$), endothermic ($+\Delta H^o$), and highly disordered at the interface of phases ($+\Delta S^o$). In addition, SFP sorbent was used well to uptake Pb ions from effluents wastewater and various water matrices.

Keywords Lead removing · Shellfish powder · Isotherm · Kinetic · Thermodynamics

Highlights
- Efficient removal of Pb(II) ions using eco-friendly shellfish powder (SFP) sorbent.
- SFP sorbent was characterized using spectroscopic and morphological techniques.
- Study the isotherm, kinetic, and thermodynamic features of the adsorption process.
- The removal mechanism of Pb(II) ions onto SFP sorbent was discussed.
- Application performance of SFP sorbent towards spiked Pb(II) ion from real water samples.

✉ Khalid M. El-Moselhy
khalidelmoselhy@yahoo.com

✉ Eman M. Saad
emmsaad@yahoo.com

1 Department of Chemistry, Faculty of Science, Suez University, Suez, Egypt

2 Department of Chemistry, Faculty of Science, Suez Canal University, Ismailia, Egypt

3 National Institute of Oceanography and Fisheries, NIOF, Cairo, Egypt

1 Introduction

Water is a vital resource for our culture. In addition to being important for life and economic growth, water is a fundamental component in the production of practically everything that keeps civilization alive, such as energy, food, clothes, automobiles, and electronics, to name a few examples. In addition to relieving our thirst, it is therefore a vital element of our life. Moreover, our future economy and security are greatly dependent on the supply of pure water. However, despite its crucial significance, the global supply of renewable freshwater is limited and there is no replacement. Population and economic expansion, urbanization, and climate change intensify the growing strain on freshwater resources. Consequently, society must immediately discover scientific and technical ways to manage our valuable water supplies more effectively.

Lead(II) ions are a hazardous metal that occurs naturally in the crust of Earth. The excessive use of lead in human actions, including fossil fuels combustion, mining, batteries, paints, and other manufacturing, increased the quantity of

Published online: 06 March 2023

lead in the environment, posing a significant danger to global public health. It is a systemic toxin that causes anemia, renal dysfunction, brain tissue damage, and even death in severe cases of poisoning. Due to the neurotoxicity of lead, kids who live with severe lead harm may be left with intellectual impairment and behavior problems [1]. Depending on the World Health Organization (WHO) recommendations, the maximal tolerable lead content in drinkable water is 0.01 mg L^{-1} [2].

Before releasing industrial wastewater effluents into the ecosystem, the rising worldwide public health concerns linked with the environmental pollution by many heavy metals motivate the development of a treatment technique capable of minimizing these metals [3]. Numerous techniques have been investigated for the development of more effective and economical technologies, either by decreasing the quantity of wastewater produced or the enhancement of the quality of effluents [4]. To eliminate metals from industrial wastewater, a variety of separation and treatment processes are routinely used. Adsorption is by far the most adaptable and prevalent approach for removing Pb and other metal ions, but ion exchange, precipitation, electro-dialysis, and reverse osmosis are also commonly utilized. Using living or nonliving bio-materials for the capturing of heavy metal from an aquatic medium is one of the more modern methods due to its broad area of target contaminants, high adsorption efficacy, eco-friendliness, and cheap rate. Several researchers have investigated this technique as a promising alternative compared with other techniques for heavy metal uptake from wastewater effluents [5–9].

Hazelnut shells, pecan shells, jackfruit, maize cob, rice husk, and husk may be utilized as toxic metal ions adsorbents [4]. In addition, researchers have used a variety of mollusk shells as natural sorbents for the capturing of metals [(10–12)]. More than 95% of molluscan shells are composed of $CaCO_3$, with tiny amounts of protein, SiO_2, and polysaccharides [13–15].

The little intertidal bivalve *Brachidontes variabilis* belongs to the Mytilidae family, Mytilida order, Bivalvia class, and Mollusca phylum. It attaches itself to rigid surfaces in the midlittoral region by abyssal filaments, generating mytilid beds that may spread enormous densities by covering a vast geographical area. Its geographic range encompasses the Red Sea, Mediterranean Sea, Indian Ocean, and western Pacific Ocean according to several reports [16–20].

The shellfish powder (SFP) of the mussel *Brachidontes variabilis* was employed as a natural, economic sorbent material for collecting lead(II) ions from aquatic medium and wastewater effluents. *B. variabilis* animals were selected as they are abundant and widely spreading in the marine coastal area and can cultivate under aquaculture conditions. In addition, their shells can easily be handled and prepared, and their powder has several advantages including being eco-friendly and low cost. In the present study, various SFP sorbent characteristics were examined to determine the best experimental circumstances. We examined the investigative kinetics, isothermal methods, and sorption process. Assessing the thermodynamic parameters (ΔH^o, ΔG^o, and ΔS^o). Also, the structural characteristics of SFP sorbent were defined.

2 Experimental

2.1 Preparation of shellfish powder

Living *Brachidontes variabilis* "*Mytilus arabicus*" mussels were gathered from the intertidal area of Egypt's northern Gulf of Suez. The creatures were moved to the laboratory in plastic containers. The shells were removed from the soft tissues, then cleaned and rinsed to remove traces of flesh. The shells were then soaked for 24 h in double-distilled water, rinsed five times with double-distilled water (DDW), and dried at room temperature for up to 48 h. The sorbent material was then dried at 100° C in an oven. The shells were ground up in a laboratory blender (Fritsch Pulverisette Mortar Grinder). The powders were sieved using a conventional set of sieves (FILTRA - Electromagnetic Sieve Shakers) to yield six distinct particle sizes (0.063, 0.125, 0.25, 0.5, 1.0, and >2.0 mm). For the following studies, the powders were subsequently stored in clean, airtight polyethylene bags [21–22].

2.2 Characterization techniques

Using a Bruker S8 Tiger X-ray Fluorescence (XRF) instrument, the powdered mussel was analyzed for its elemental structure. On a Bruker FT/IR Alpha-II, FT-IR spectra were scanned. The X-ray diffraction (XRD) investigations are performed using an XRD Siemens D5000 powder diffractometer equipped with Cu Kα radiation ($\lambda = 0.15406$ nm), a Ni-filter, 30 mA, and 40 kV. The diffractometer was run within the 2θ range of (10°–100°) by using a step size of 0.05°/s. Japan's JEOL JSM 6510-V electron microscope was used for transmission electron microscopy (TEM). The scanning electron microscope (SEM) with energy-dispersive X-ray (EDS) measurement was conducted with a Field-Emission Scanning Electron Microscopy (model FESEM, Zeiss SEM Ultra 60, 5 kV) and an Energy Dispersive Analysis System of X-ray (Oxford). Pb(II) concentrations were evaluated by a flame atomic absorption spectrophotometer (AAS-Perkin Elmer, model Analyst 100) to quantify Pb (II).

2.3 Sorption tests

Set sorption investigates were conducted to determine the influence of several factors, including contact time (5–180 min), sorbent particle size (0.063–2.0 mm), pH (2–7), initial concentration of Pb(II) (13–680 ppm), quantity of sorbent (0.01–0.5 g), temperature (10–40 °C), and agitation rate (100–500 rpm), on sorption investigations. Using Whatman No. 1 filter paper, the adsorbate was separated from the sorbent, and the experimental conditions were altered based on the investigated factor. By using the next equations (1–3), the lead removal efficacy (%) and capturing capacity (mg g^{-1}) were computed at equilibrium and time *t*:

$$\text{Pb removal (\%)} = \frac{C_o - C_e}{C_o} \times 100\% \quad (1)$$

$$q_e = \left(C_o - C_e\right)\frac{V}{m} \quad (2)$$

$$q_t = \left(C_o - C_t\right)\frac{V}{m} \quad (3)$$

where q_t (mg g^{-1}) and q_e (mg g^{-1}) are the sorption capacities at time *t* and equilibrium, respectively, where the sorption and desorption rates become identical. Similarly, C_t and C_e (mg L^{-1}) led (II) concentrations at time *t* and equilibrium conditions. C_o, *m*, and *V* are the initial lead (II) concentration (mg L^{-1}), the adsorbent's mass (g), and the volume of solution (L), respectively.

Sorption isotherm was examined by differing initial Pb ions solution concentrations (13–680 mg L^{-1}). Suspension of 0.05 g SFP and 50 mL of solution was agitated at 250 rpm shaking rate; pH 5.5, at temperature 25° C, using < 0.063 mm SFP particles size for 90 min were sufficient to attain equilibrium condition [23, 24].

2.4 Applications

Industrial wastewater "obtained from the Adabiya wastewater treatment plant, Gulf of Suez, Egypt," tap water, different percentages of seawater (25, 50, 75, and 100%), and deionized water (DIW) were used to assess the ability of SFP sorbent in removing Pb(II) ions, under optimization conditions (90 min contact period, pH 5.5, 130 Pb mg L^{-1}, 0.05 g of SFP sorbent, 250 rpm, and 0.063 mm SFP particles size at 25 °C), in 50 mL solution. As a control, DIW having the same quantity of Pb(II) was generated for determining the effect of industrial effluent and seawater components on Pb(II) capturing.

3 Results and discussion

3.1 SFP sorbent characterizations

XRF indicated that the processed clam powder had 50.29% CaO, 0.24% SiO_2, 0.53% Al_2O_3, 0.16% MgO, 0.35% SO_3, 0.01% K_2O, 0.22% Na_2O, 0.05% P_2O_5, 0.01% TiO_2, 0.01% MnO_3, and 48.3% LOI (loss of ignition). Accordingly, the SFP (unloaded and loaded Pb ions) composition was scanned using EDS, which proved the existence of Ca, O, C, Mg, Na, K, Al, Si, S, and P in its structure and accompanied the capture of Pb(II) ions on the SFP sorbent (Fig. 1). The TEM micrographs of *B. variabilis* shell powder (Fig. 1a) indicated that its surface is uneven and heterogeneous [22, 25]. The observed considerable changes in the particle size of the SFP sorbent after lead adsorption verified the replacement of lead ions in carbonate phase lattice via ion exchange mode (Fig. 1b), as well as the lead(II) ion adsorption from aquatic solutions onto SFP particles [26]. Previously, many investigations have studied this behavior using aquatic sorbents after metal sorption [22, 27–32]. In this context, the color of the SFP powder slightly changed after Pb loading from beige to slightly dark beige (Fig. 1e and 1f). SEM scans of the current sorbent revealed two distinct sections (dark and white zones). The black regions are mostly composed of proteins having high concentrations of oxygen, carbon, and sulfur, while the white portions are often composed of inorganic compounds holding high concentrations of phosphorus and calcium [33–34].

EDS pattern of the raw SFP surface demonstrated the lack of the distinctive Pb(II) peak (Fig. 1c), while SFP-loaded Pb(II) ions presented the characteristic Pb(II) peak (Fig. 1d), demonstrating the presence of lead on the SFP surface [22]. In general, the presence of Pb-specific post-sorption peaks shows the linkage of metal ions with the sorbent surface. Accordingly, based on the findings of the EDS examination, there are influential and plausible reasons for Pb ions capturing by the SFP sorbent [35]. The amount of the sorbed metals correlates directly with the intensity of respective EDS signals [36]. In addition, the Pb ions percent loaded onto the sorbent surface is around 3.6%, which replaced the principal cations (Ca, Mg, K, and Na), particularly Ca, which was reduced by 3.4% (Fig. 1b). To confirm this phenomenon, the level of the major cations was measured using an atomic absorption spectrophotometer in the samples of the sorption experiment conducted under optimum conditions versus the control, confirming the presence of Ca and Mg in the solution after the removal process by approximately 1.98 and 0.03%, respectively, and a concurrent decrease in their level in EDS. This study suggested that Pb ions can substitute for the main components Ca and Mg.

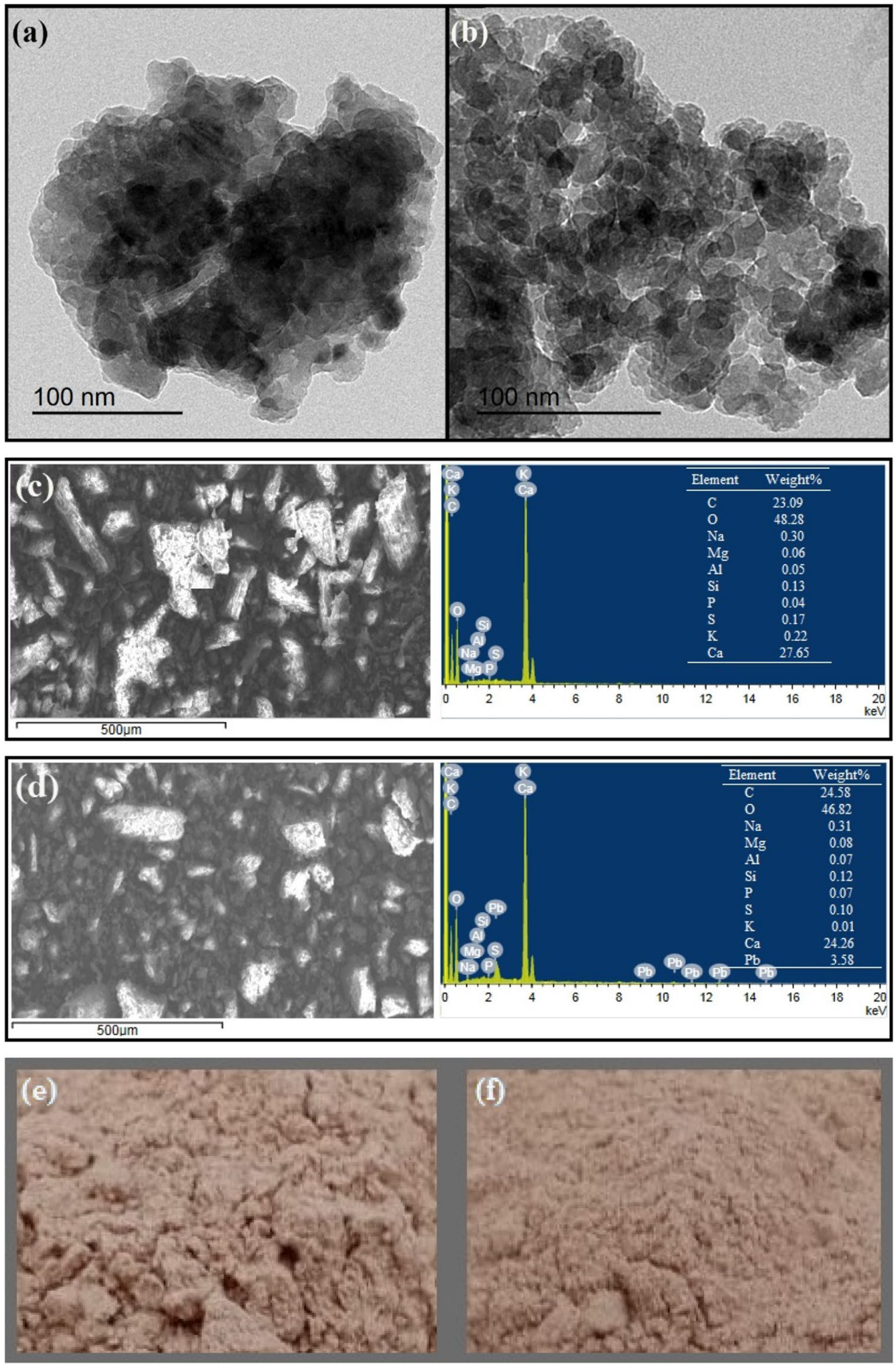

Fig. 1 TEM images before (**a**) and after (**b**) Pb ions sorption; SEM images and corresponding EDS spectra before (**c**) and after (**d**) Pb ions sorption; and powder of the SFP sorbent before (**e**) and after (**f**) Pb ions sorption. Inserts: Elemental composition (weight %)

The clam powder was analyzed by FTIR spectroscopy before and after Pb adsorption (Fig. 2a and b). The C–O stretching of $CaCO_3$ assigned three different vibrational bands at $710.94_{(s)}$, $857.54_{(m)}$, and $1451.04_{(s)}$ cm^{-1}, and the band at $1081.08_{(l)}$ cm^{-1} is associated with the symmetric mode of carbonate ion [37]. After the adsorption of Pb, the band peaks move slightly to 709.29, 857.18, 1080.76, and 1447.08 cm^{-1}, respectively. However, the difference between these bands may result from the replacement of Pb ions on the SFP sorbent [22].

Figure 3 shows the XRD patterns of raw SFP and loaded Pb(II)-SFP. The figure exhibits 16 typical peaks

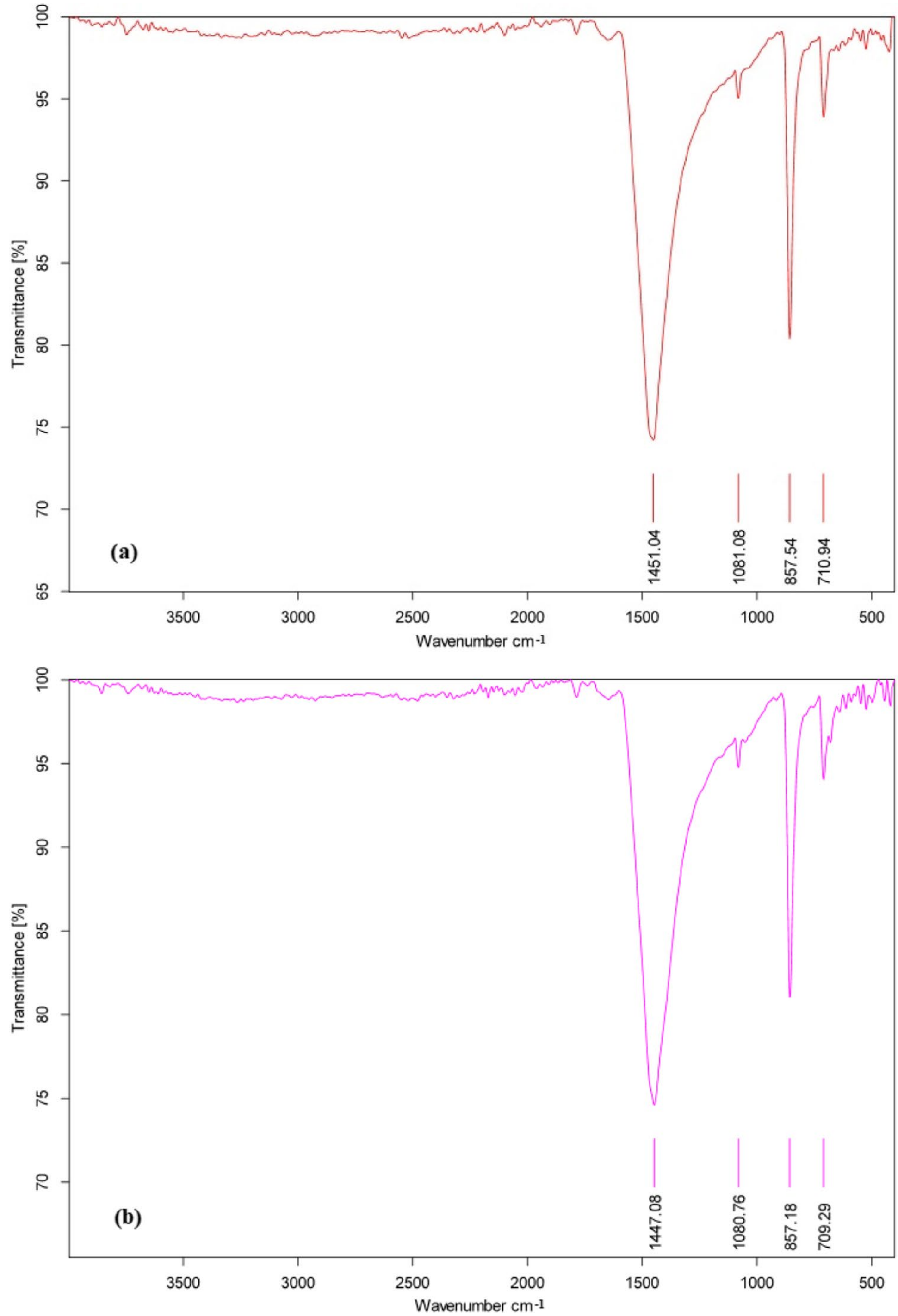

Fig. 2 IR spectra of SFP sorbent before (**a**) and after (**b**) loading Pb (II) ions

organized at 2θ between 26.0° and 53.0° for the raw SFP, indicating full agreement of shellfish powder with aragonite $CaCO_3$ [37] with a minimal amount of other elemental components. New peaks at 2θ (20.95°, 24.85°, and 34.30°) were found in the loaded SFP after the adsorption procedure, which may be related to the presence of Pb ions.

3.2 Batch capture of Pb(II)

3.2.1 Influence of contact time

Time of adsorption is crucial for achieving maximal metal removal capability in water treatment operations [38]. In this investigation, Pb(II) ion absorption increased

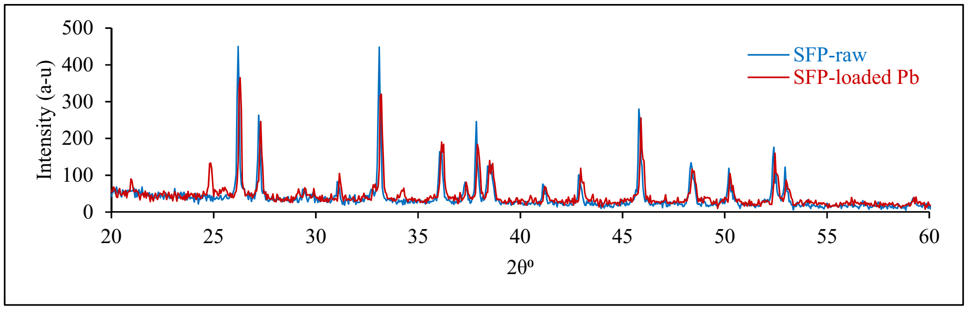

Fig. 3 X-ray diffraction of raw SFP (**a**) and SFP-loaded Pb(II) (**b**)

progressively over 90 min to approach equilibrium (Fig. 4a). In the subsequent sorption experiments, the equilibrium contact period was thus established at 90 min. The impact of contact time on capturing Pb(II) onto SFP sorbent was simulated by varying the starting concentrations of Pb ions (130, 260, and 520 mgPb L^{-1}). The obtained data demonstrated that the SFP sorbent removed nearly all of the Pb ions from concentrations of 130 and 260 mgPb L^{-1} at sorption capacities of 129.38 and 259.21 mg g^{-1}, respectively, and removed approximately 50% from a solution of 520 Pb mg L^{-1} at a capturing capacity of 259.87 mg g^{-1} and reached equilibrium at 90 min (Fig. 4b). This result indicated that the researched sorbent (powdered shells of the mussel *B. variabilis*) could remove Pb ions from aqueous solution at a maximum sorption capacity of about 260 Pb mg g^{-1} sorbent under the optimal conditions mentioned in the current study.

3.2.2 Influence of particle size of SFP sorbent

To determine the optimal size of the SFP particle for the adsorption equilibrium, a constant quantity of 0.05 g of SFP sorbent of various sizes of the particle (0.063 to > 2.0 mm) was introduced to 50 mL of 130 Pb mg L^{-1}, contact period of 90 min at 25 ºC, agitation rate of 250 rpm and pH of 5.5. Figure 5 depicts the influence of SFP sorbent particle size on the capturing efficacy of Pb(II) from an aqueous solution by SFP sorbent. A notable drop in Pb (II) sorption efficacy was marked when the size of the particle increased from 0.063 to > 2.0 mm. Fine particles (silt and clay) had the higher removal percentage (~ 99.5%), whereas other particle sizes (0.125–> 2.0 mm) had percentages ranging from 63.83 to 37.05 %. The greater uptake percentage obtained with smaller sizes of the SFP particle might be attributable to the fact that smaller particles had the highest specific surface area for removal, while as surface area decreased, the size of the particle increased [39, 40]. Due to the reduced particle size, the fragmentation of larger particles tends to create minute fissures and channels on the SFP surface, causing a greater surface area available for diffusion [41]. The size of a particle of 0.063 mm was preferred for the following trials owing to its high adsorptive performance relative to other SFP particle sizes.

3.2.3 Influence of pH

Due to its impact not only on the reactivity of adsorptive sites on sorbents but also on the chemistry of metal in the solution, pH value has a significant effect on adsorption investigations [42]. The uptake of Pb(II) by SFP sorbent at pH values ranging from 2 to 7 was investigated for determining both its effect on the capturing effectiveness and the optimal pH value for Pb(II) uptake. The findings demonstrated that the Pb(II) sorption increased with the pH of the solution until it attained a maximum at 5.5 and then reduced slowly until pH 7 (Fig. 6). From the 3 to 6 pH range, the adsorption capacity increased owing to a decrease in the competitive H^+ ion action on Pb(II) and the increase in solubility of the sorbent, resulting in enhanced sorption. At pH values above 7, insoluble $Pb(OH)_2$ precipitated [43]. Therefore, pH 5.5 was optimal for the following sorption tests of the SFP sorbent.

3.2.4 Influence of initial concentration of Pb(II) ion

The quantity of metals removed is greatly depending on the starting level of metal ions. Figure 7 depicts the influence of starting Pb concentrations in the range of 13 to 680 mg L^{-1} on the sorption process under the suggested conditions. According to the adsorption capacity, the capturing of Pb(II) ions increased as the starting concentration of Pb(II) increased, reaching an equilibrium point at around 260 mg L^{-1} Pb ions. Regarding the Pb percent removal, Pb ions were eliminated (~ 99%) from 260 mg L^{-1} initial Pb concentration solutions and thereafter dropped to around 38 % in a 680 mg L^{-1} Pb solution. This may be because the amount of Pb ions was higher than the number of active sites accessible for removal, resulting in rapid initial absorption of Pb ions at the sorption process' onset [44, 45]. Consequently, 130 mg L^{-1} Pb was preferred for future sorption experiments of SFP sorbent.

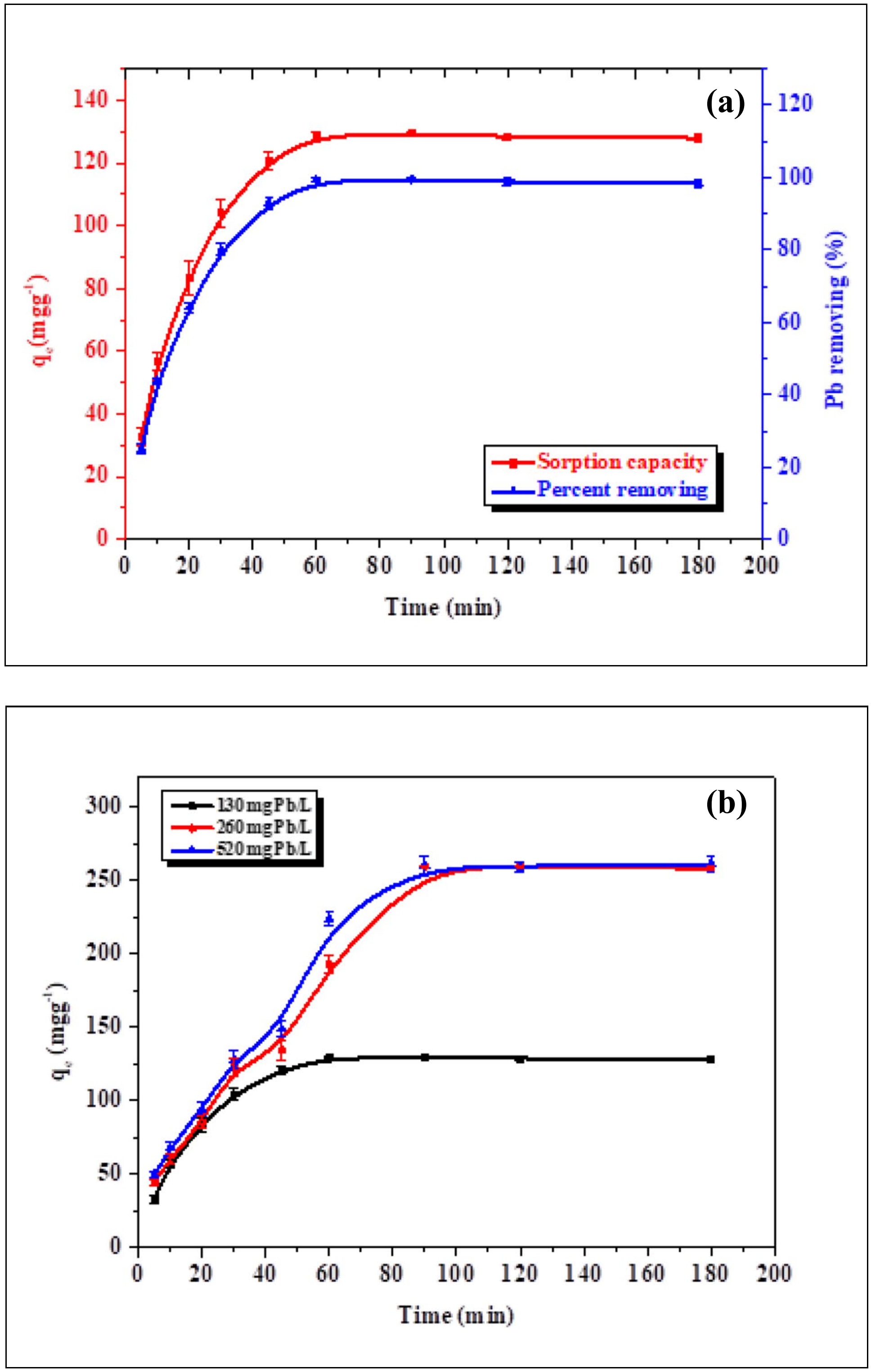

Fig. 4 **a**, **b** Influence of contact duration on the sorption of Pb(II) by SFP sorbent at different concentrations (130, 260, and 520 mg L^{-1})

3.2.5 Influence of SFP dosage

The quantity of SFP sorbent is a crucial variable in treatment research [46, 47]. Owing to the larger availability of Pb binding adsorptive sites of the surface area of SFP sorbent at higher amounts of adsorbent [24, 48], the capturing efficacy of Pb(II) ions, in the current experiment, increases with rising sorbent dosage and decreasing adsorption capacity (Fig. 8). Consequently, 0.05 g SFP sorbent was used in the subsequent batch removal studies.

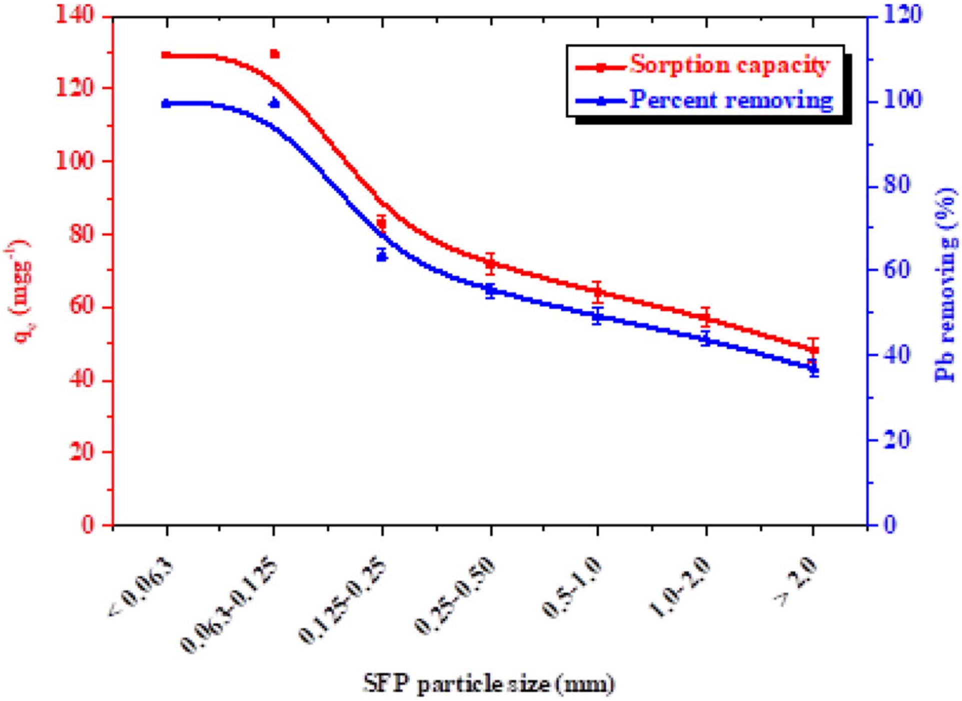

Fig. 5 Influence of the size of the particle on the capturing of Pb(II) ions by SFP sorbent

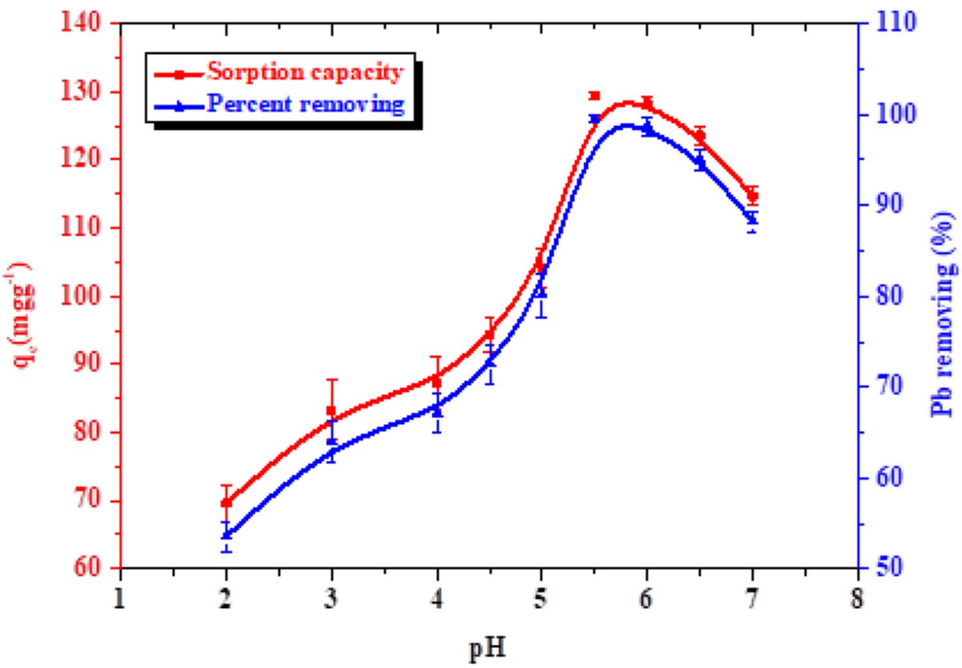

Fig. 6 Influence of pH on the adsorption of Pb(II) by SFP sorbent

3.2.6 Influence of temperature

Temperature parameter has a considerable impact on the removal process and is one of the major crucial factors for the effective sorption of heavy metal ions from aquatic systems. Figure 9 shows the elimination of Pb(II) by the SFP sorbent between 10 and 40 degrees Celsius. At 25 and 30 °C, the greatest removal efficiency of Pb ions was 99.52 and 99.19%, respectively, with 129.38 and 128.95 mg g^{-1} of Pb sorption capacity. The elimination efficiency then decreased when the temperature rose over 30° C. With rising the temperature up to 30° C, it is known that the diffusion rate of adsorbate molecules inside pores increases due to a decrease in solution viscosity, and that the equilibrium capturing capacity of SFP sorbent for a specific adsorbate also modify. This is often owing to the aggregation of SPF particles at higher temperatures (above

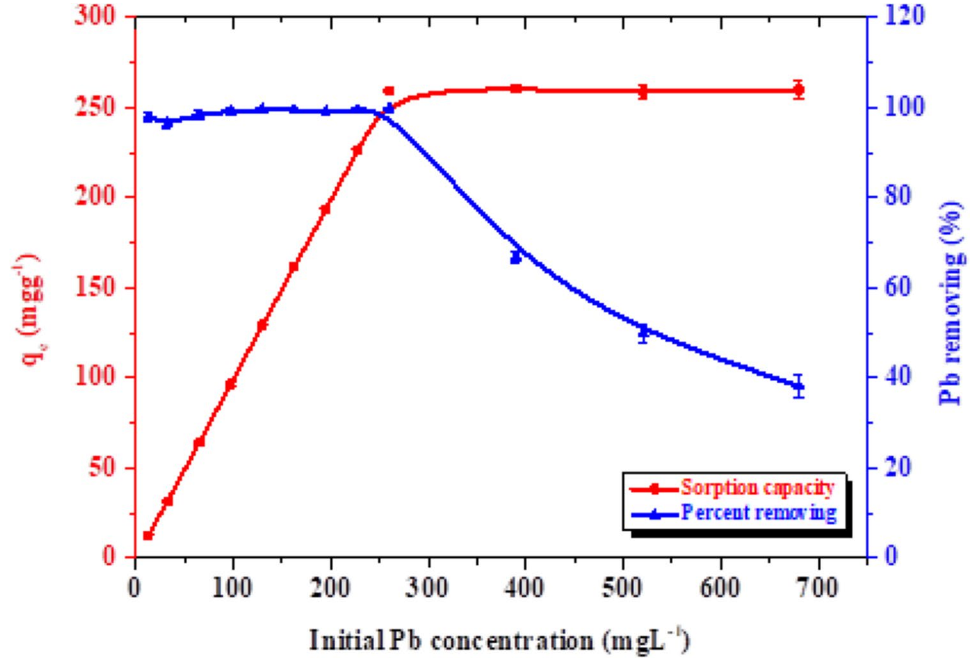

Fig. 7 Influence of initial concentration on the sorption of Pb(II) by SFP sorbent

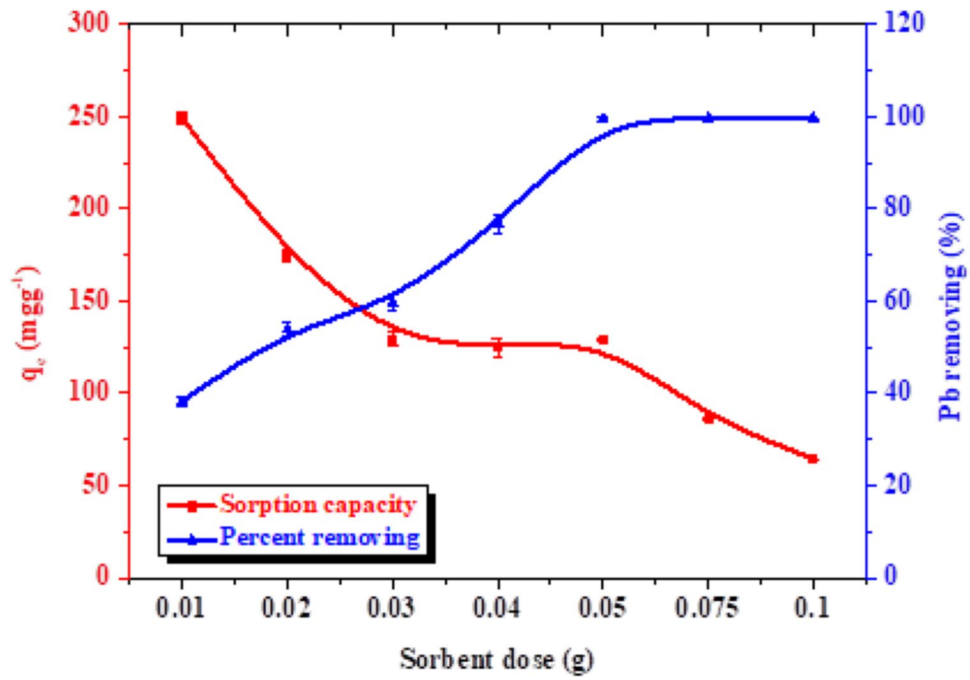

Fig. 8 Influence of sorbent amount on the adsorption of Pb(II) by SFP sorbent

30° C) and the reduction in surface activity [49, 50]. Therefore, temperatures between 25 and 30° C were preferred for the uptake of Pb from various aquatic environments.

3.2.7 Influence of the rate of agitation

The rate of agitation is a crucial element in the sorption phenomenon, as it impacts the spreading of the adsorbate in the bulk phase and the creation of the exterior boundary layer. In general, the elimination rate of ions is impacted by the agitation rate, and metal absorption increased as the stirring rate rose [51]. Figure 10 illustrates the impact of agitation rate on Pb ion sorption. The design of the agitation curve indicates a small increase in Pb(II) removal as agitation speed increases. However, after 250 rpm there is no increment. With increasing agitation rate, the potential sorption rises until it reaches

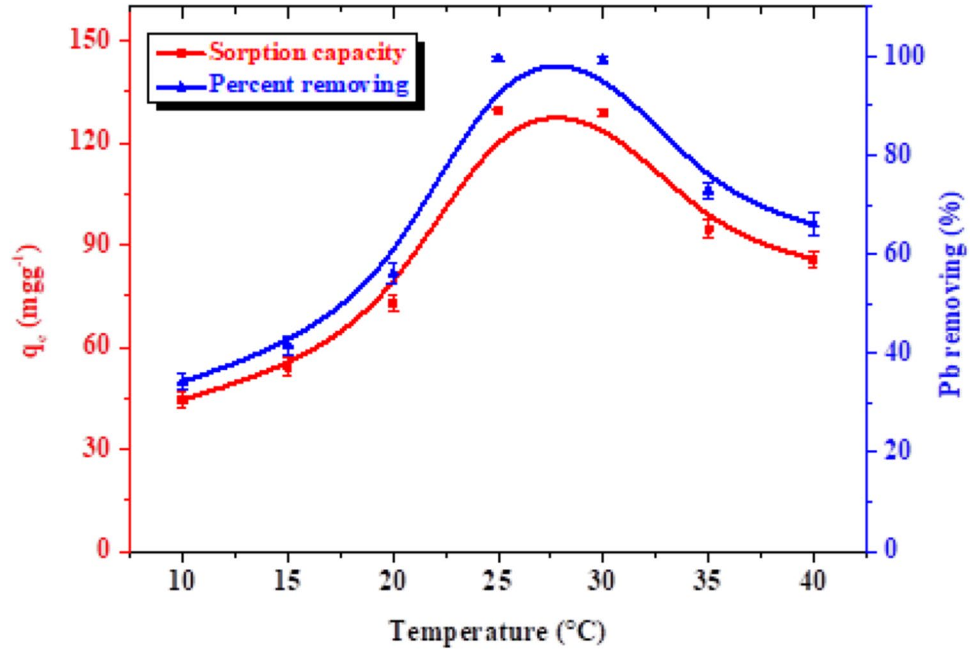

Fig. 9 Influence of temperature on the capturing of Pb(II) by SFP sorbent

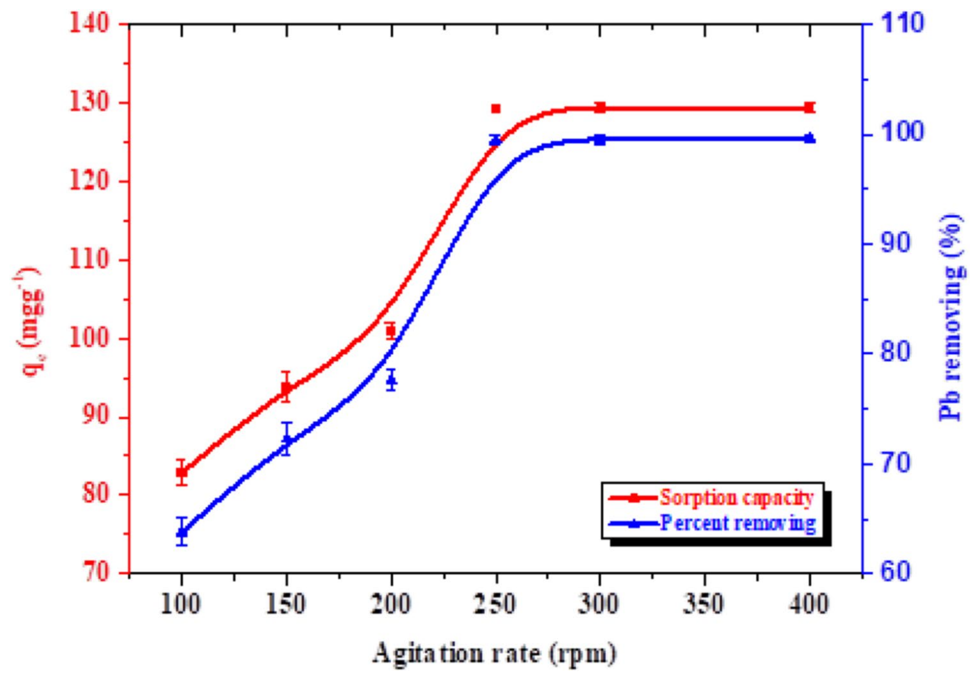

Fig. 10 Influence of agitation rate on the capturing of Pb(II) by SFP sorbent

a rate limit beyond which there is no meaningful change [51]. As a result, the optimal agitation rate was found to be 250 rpm, which was used in further tests.

3.2.8 Equilibrium isothermal models

Isothermal models may give information on the interaction performance of sorbent in the removal technique. This work gathered sorption equilibrium data for four well-known sorption isothermal models, namely Freundlich, Langmuir, Dubinin-Radushkevich (D-R), and Temkin.

The Langmuir isothermal model permits monolayer adsorbate coverage on a homogenous adsorbent surface. Adsorption of each molecule on the surface of the sorbent has the same adsorption activation energy; each molecule may occupy just one adsorptive site without forming an interface with other adjacent adsorbed molecules or atoms

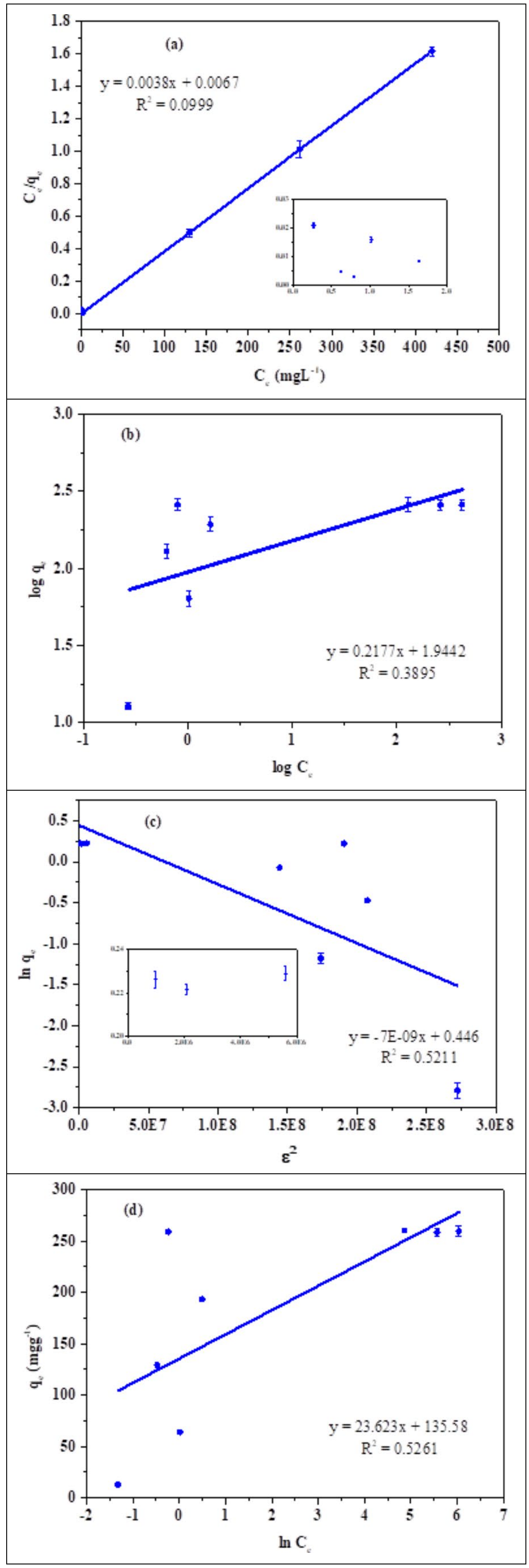

Fig. 11 Sorption isothermal models: **a** Langmuir, **b** Freundlich, **c** ▸ D-R, and **d** Temkin for the sorption of Pb(II) ions onto SFP sorbent

[52, 53]. The Langmuir isothermal formula is derived from Eq. (4):

$$\frac{C_e}{q_e} = \left(\frac{1}{q_{\max}}\right)C_e + \frac{1}{q_{\max}\mathrm{b}} \quad (4)$$

where q_{max} (mg g^{-1}) is the maximal amount of Pb (II) per weight unit of adsorbent, and *b* is the Langmuir constant (Lmg^{-1}).

The linearized relation of C_e/q_e vs C_e in Fig. 11a was constructed to calculate the maximum adsorbed quantity (q_{max}) and Langmuir binding constant (*b*), and the values of corresponding parameters are listed in Table 1.

Dimensionless constant separation factor (R_L) is a necessary characteristic of monolayer Langmuir isothermal; it can be defined by formula (5).

$$R_L = \frac{1}{1 + \mathrm{b}C_o} \quad (5)$$

Depending on the value of R_L, the nature favorability of the sorption may be quantified: for favorable adsorption, $0 < R_L < 1$; for unfavorable adsorption, $R_L > 1$; and for irreversible adsorption, $R_L = 0$: for linear adsorption, $R_L = 1$ [24, 52].

Figure 12 reports the influence of the initial concentration of Pb(II) on the separation factor (R_L) for the SFP sorbent. The acquired results confirmed that the values of R_L ranged from 0.0026 to 0.119, demonstrating the favorable capturing of Pb(II) by the SFP sorbent used in the current investigation. The R_L value approaches zero as C_o increases, suggesting less favorable adsorption at high Pb(II) ion concentrations [54].

Freundlich isothermal assumes a heterogeneous adsorbate distribution on a heterogeneous surface of sorbent (binding sites are not equivalent) and/or a multilayer sorption model [24, 52]. The Freundlich isothermal relationship is expressed by the next formula:

$$\mathrm{Log}\ q_e = \log \mathrm{K_f} + \frac{1}{n_f}\log C_e \quad (6)$$

where K_f is the Freundlich isothermal constant (mg g^{-1}), and n_f is the sorption intensity that is associated with the affinity of Pb(II) on the SFP sorbent.

The linear plot of the Freundlich model is determined by graphing log q_e versus log C_e (Fig. 11b). From the slope and intercept, the Freundlich parameters n_f and K_f were computed. Freundlich constant (K_f) demonstrates the adsorption ability of the heterogeneous surface of non-uniform available sites with diverse energies which might

Table 1 Sorption isothermal models for capturing Pb(II) ions onto SFP sorbent

Isotherm model	
Experimental q_e (mgg^{-1})	259.21
Langmuir	
q_{max} (mgg^{-1})	263.16
b (Lmg^{-1})	0.5672
R^2	0.9999
Freundlich	
K_f (mgg^{-1})	87.943
n_f	4.594
R^2	0.3895
D-R	
q_m (mgg^{-1})	323.66
E ($kJmol^{-1}$)	8.339
R^2	0.5211
Temkin	
A	310.85
B	23.623
R^2	0.5261

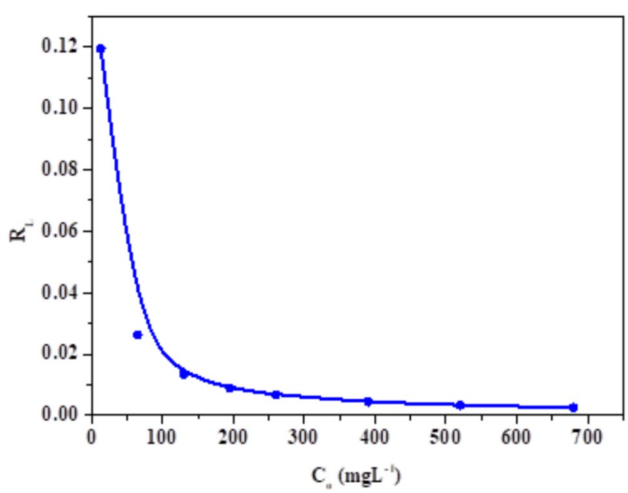

Fig. 12 Plot separation factor (R_L) as a function of starting Pb(II) ions concentration

assist as an indication of the maximal metal ion (Pb) capturing capacity of SFP sorbent. The sorption intensity (n_f) represents the affinity of Pb(II) toward the SFP sorbent, and n_f value indicates the adsorption favorability. According to Goldberg [55] and Saad et al. [56], the sorption process is favorable at n_f value is ≥ 1. Table 1 illustrates Freundlich isothermal parameter values; K_f, n_f, and regression coefficient (R [2]). Therefore, Freundlich isotherm is less applicable to SFP sorbent.

The Dubinin-Radushkevich (D-R) model is applicable to differentiate between chemisorption and physisorption processes based on the level of sorption energy [52, 57]. The linearized plot of the D-R isothermal is pronounced by Eq. (7):

$$\ln q_e = \ln q_m - \beta \varepsilon^2 \tag{7}$$

where q_e (mol g^{-1}) is the quantity of lead (II) sorbed per unit dose of the sorbent, q_m (mol g^{-1}) is the theoretic monolayer-sorption capacity, and β (mol [2]J^{-2}) is sorption energy, which is correlated to the mean energy of sorption per mole of Pb(II), and ε is the Polanyi potential, ε is defined by Eq. (8):

$$\varepsilon = RT \ln\left(1 + \frac{1}{C_e}\right) \tag{8}$$

where T is the solution temperature (K), and R (8.314 $Jmol^{-1}K^{-1}$) is a gas constant.

The mean sorption energy (E - $kJmol^{-1}$) is computed from parameter β of D-R (Eq. 9).

$$E = \frac{1}{\sqrt{-2\beta}} \tag{9}$$

The linear graph of the D-R isothermal model for Pb(II) ions is shown in Fig. 11c, and the level q_m, mean sorption energy (E), and regression coefficient (R [2]) were estimated and tabulated in Table 1. According to the D-R model, the value of β was utilized to compute the mean bonding energy (E, $kJmol^{-1}$) from Eq. 9. If the value of E lies between 0-8 kJ mol^{-1}, the sorption process is stated to physic-sorption; if E is between 8-16 $kJmol^{-1}$, the sorption agrees with ion exchange process; and if E is >16 $kJmol^{-1}$, the sorption matches with chemi-sorption [58]. Therefore, findings in Table 1 (E is 8.339 $kJmol^{-1}$) show that the sorption of Pb(II) by SFP may be governed by an ion exchange process. In addition, the D-R model agreed with the Langmuir model analysis, indicating that the sorption process followed monolayer adsorption.

Temkin isothermal consists of a component that explicitly takes into account interactions of sorbent-adsorbate [24, 52, 59]. Due to sorbent-adsorbate interactions, the adsorption heat of all molecules in the layer would linearly decrease with increasing coverage. Up to maximum binding energy, the sorption is characterized by an equal distribution of binding energies. The Temkin isothermal formula is shown in Eq. (10) as follows:

$$q_e = B \ \ln \ A + B \ \ln \ C_e \tag{10}$$

where $B = RT/b_{te}$ refers to the constant of Temkin which is associated with sorption heat ($Jmol^{-1}$), A is the binding constant at equilibrium parallel to the maximal energy of binding (Lg^{-1}), T is the Kelvin temperature solution (K), and R (8.314 $Jmol^{-1}K^{-1}$) is the ideal gas constant.

For the Temkin isothermal graph of q_e vs ln C_e (Fig. 11d and Table 1), the constant of equilibrium binding ($A - Lg^{-1}$) equivalent to the maximal binding energy and Temkin constants values ($B - Jmol^{-1}$) linked to the sorption heat and were determined from the intercept and slope, respectively [52]. In accordance with the regression coefficient (R [2]), it is evident that the Temkin isothermal model fits the SFP sorbent less well.

According to the currently examined isotherms, the Langmuir isothermal model is connected with the experimental equilibrium results from the sorption equilibrium of Pb(II) by SFP sorbent better than the other models, showing monolayer adsorption. Langmuir isothermal model is the best fitting for the sorption lead ion process with greater regression coefficients ($R^2 = 0.9999$), and the sorption maximum capacity (q_{max}) of 263.16 mg g^{-1} is close to the investigational sorption capacity (q_e) of the sorption process (259.21 mg g^{-1}).

3.2.9 Sorption kinetics

To illustrate the uptake rate and sorption process of Pb(II) ions by the SFP sorbent, Fig. 13a, b and c present the kinetic model's quasi-1st order, quasi-2nd order, and intra-particular diffusion.

For the quasi-1st order model, the rate of the adsorptive interaction can be designed by the Lagergren equation (Eq. 11) [24, 53, 60, 61]. k_1 and q_e are found by graphing log (q_e-q_t) against t (Fig. 13a and Table 2). Based on q_e (234.91) and R^2 (0.913) values, the quasi-1st order model for the capturing of Pb ion by SFP sorbent was well fitted.

$$\log\left(q_e - q_t\right) = \log q_e - \left(\frac{k_1 t}{2.303}\right) \tag{11}$$

where k_1 is the 1st order rate constant (min^{-1}).

Quasi-2nd order model is formulated by equation (12) [24, 62]. k_2 and q_e were acquired from the intercept and slope, respectively, of the straight graph of t/q_t vs t (Fig. 13b and Table 2). The quasi-second order model ($R^2 = 0.747$) could not match the kinetics as well as those achieved by the quasi-first order kinetics model where the high linearity of the plot versus t ($R^2 = 0.913$) confirmed that the nature of the sorption process follows quasi-1st order.

$$\frac{t}{q_t} = \frac{1}{k_2 q_e^2} + \frac{1}{q_e} t \tag{12}$$

where k_2 is the 2nd order constant (gm $g^{-1}min^{-1}$).

Intra-particle diffusion (IPD) model [24, 52] was utilized for the results of kinetic practical to view the rate-determining steps and is useful for elucidating the adsorption process. The IPD model is defined as follows (Eq. 13):

$$q_t = k_{ipd} t^{0.5} + c \tag{13}$$

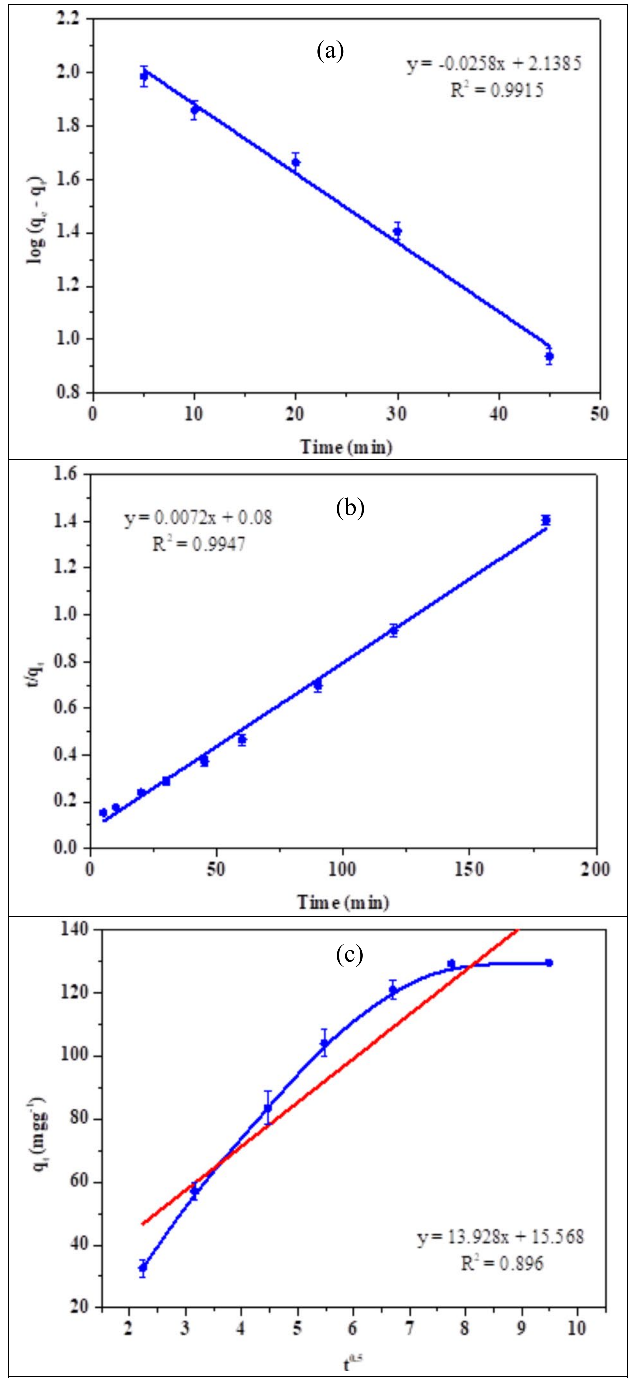

Fig. 13 Sorption kinetic models: **a** quasi 1st order, **b** quasi 2nd order, and **c** intra-particular diffusion of Pb(II) ions onto SFP sorbent

Table 2 Equilibrium kinetics models for the sorption of Pb(II) ions onto SFP sorbent

Sorbent	Experimental q_e (mgg^{-1})	Equilibrium kinetics model								
		Pseudo-1st order			Pseudo-2nd order			Intra-particle diffusion		
		k_1	q_e (mgg^{-1})	R^2	k_2	q_e (mgg^{-1})	R^2	k_{ipd}	$C(mgg^{-1})$	R^2
SFP sorbent	259.21	0.0101	234.91	0.913	2.80E^{-05}	400.0	0.747	27.7	49.7	0.894

Table 3 Thermodynamic functions for sorption of Pb(II) by SFP sorbent

Temperature (K)	ΔG^o (kJmol^{-1})	ΔH^o (kJmol^{-1})	ΔS^o (kJmol^{-1}K^{-1})	R^2
283.15	1.53	236.2	0.822	0.794
288.15	0.80			
293.15	-0.60			
298.15	-13.24			
303.15	-12.12			

where k_{ipd} is the intra-particle diffusion rate constant (mg·g^{-1}·min$^{-0.5}$), $t^{0.5}$ is the square root of shaking time, and C is the boundary layer effect that increases with the increasing temperature of the solution.

Figures 13c and Table 2 show the graphs of q_t versus ($t^{0.5}$) attained from the adsorption of Pb(II) by SFP sorbent. Equation (13) was used to obtain the intra-particular rate constant k_{ipd} (mgg^{-1}min$^{-0.5}$) and intercept C. Three separate steps are involved in the sorption of Pb(II), as seen by the non-linear graphs across the complete time range. These steps include (i) the migration of sorbate species to the outer sorbent surface (film diffusion); (ii) diffusion of sorbate into the pores in the sorbent structure (particle diffusion); and (iii) the sorption on the outer surface of the sorbent. When IPD is the primary rate-determining stage, the graph must be centered on the origin; otherwise, boundary layer diffusion influences sorption to some extent. Our observations revealed that IPD is not the sole rate-determining variable [24, 52].

3.2.10 Sorption thermodynamics study

To explain the thermodynamic features of the adsorption processes, tests were accompanied at varied temperatures (10, 15, 25, and 30 °C), with an initial concentration of Pb (130 mg L^{-1}) and 0.05 g SFP sorbent. Thermodynamically parameters (Table 3) as standard enthalpy change ΔH^o (kJmol^{-1}), Gibbs free energy ΔG^o (kJmol^{-1}), and standard entropy change ΔS^o (kJmol^{-1}K^{-1}) were elaborated from the thermodynamic distribution coefficient based on the following formulas (14–16) [24, 53, 63].

$$\Delta G^o = -RT \ln \mathrm{K_d} \tag{14}$$

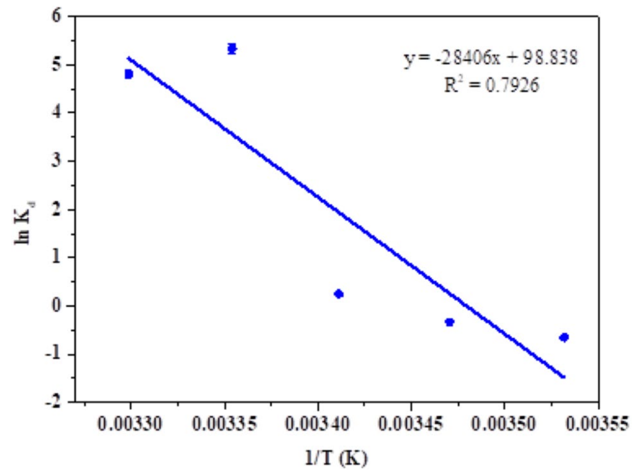

Fig. 14 Thermodynamic plot of Pb(II) sorption by SFP sorbent

$$\mathrm{K_d} = \frac{C_{\mathrm{ads}}}{C_{\mathrm{e}}} \tag{15}$$

$$\ln \mathrm{K_d} = \frac{\Delta S^o}{\mathrm{R}} - \frac{\Delta H^o}{\mathrm{R}T} \tag{16}$$

where K_d is the distribution equilibrium constant and represents the concentration ratio of lead ion in the solid phase (C_{ads}) to the aqueous phase (C_e) at equilibrium (mg L^{-1}), T is the temperature in Kelvin (K), and R is the gas constant (8.314 Jmol^{-1}K^{-1}).

The adsorption experiment was operated at assorted temperatures to get a deeper insight into the sorption process of Pb onto SFP sorbent. The equilibrium Pb(II) sorption capacity of SFP elevates with the elevation in temperature, positing that the sorption process is endothermic (Fig. 14). To further scrutinize the sorption process, thermodynamically parameters, including Gibbs free energy (ΔG^0, kJ/mol), standard enthalpy (ΔH^0, kJ/mol), and standard entropy (ΔS^0 J/mol K), were reckoned via the Eqs. 14–16. The slope and intercept of the linear plot of ln K_d against 1/T were used to elicit the ΔH^0 and ΔS^0 values, while ΔG^0 was computed from Eq. (14). The negative sign of ΔG^o refers to the spontaneity of adsorption process while the positive signs of ΔH^0 and ΔS^0 refer to endothermic nature and rising the disorder degree of Pb(II) at the interfaces of solid/liquid, respectively [39, 64].

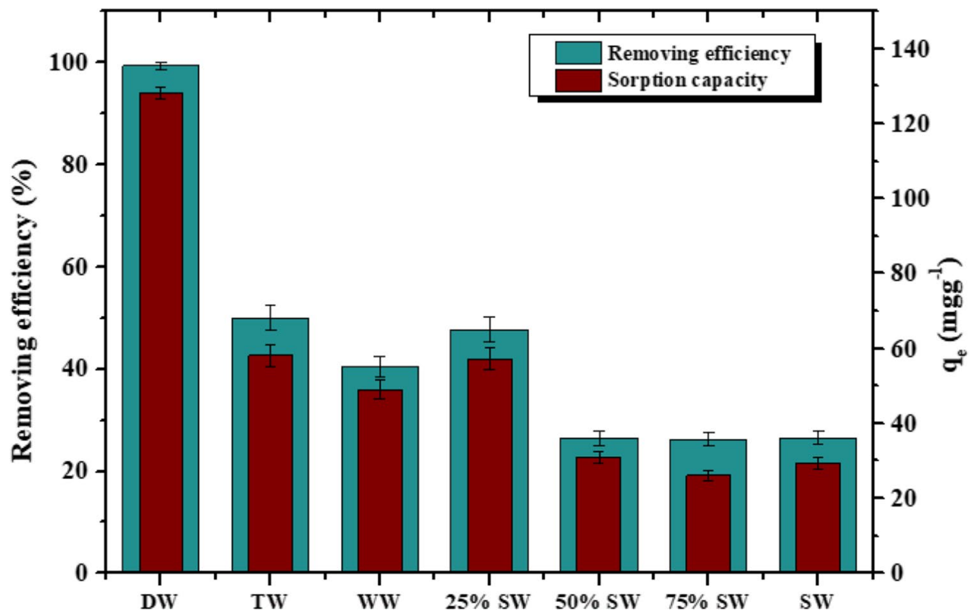

Fig. 15 Removal efficacy of Pb(II) from various water types (DW: deionized water; TW: tap water; WW: wastewater; SW: seawater)

3.3 Removal mechanism

To gain further insight into the sorption mechanism from the experimental results, Pb(II) indeed changed the structure during the adsorption process. Based on the TEM micrograph, the morphology changed from micro-scale aggregates to nano-scale irregular spheres after the adsorption of Pd(II), i.e., an increase in the surface area [65]. Also, according to EDS data, Pb(II) ions percent loaded onto the sorbent surface is ~ 3.6%, replacing Ca(II), Mg(II), K(I), and Na(I) cations, particularly Ca(II), which reduced by 3.4%. This phenomenon is confirmed by the measurement of the level of the major cations by atomic absorption spectrophotometry in the samples of the sorption experiment conducted under optimum conditions versus the control. The obtained result approved the presence of Ca(II) and Mg(II) in the solution after the removal process by approximately 1.98 and 0.03%, respectively, and a concurrent reduction in their level in EDS. This study suggested that Pb(II) ions may substitute for the main components Ca(II) and Mg(II). In addition, the D-R model agreed with the Langmuir model analysis, indicating that the sorption process followed monolayer adsorption with mean adsorption energy value (8.34 kJ mol^{-1}) indicating ion exchange adsorption process. Thus, the removal capacity of SFP is depending on the optimal exchange of Pb(II) with the adsorbent and dominated driving force during the removal process.

3.4 Applications

Several attempts were made to adapt the aforementioned sorption experimental findings to actual water types so that they may be implemented in the real world. Under optimal circumstances, the removal efficiency of the SFP sorbent for Pb(II) ions from various water types (tap water, waste water, sea water “25, 50, 75, 100 %” with varying percent to tap water, and deionized water as a control) spiked with Pb(II) ions (130 mg L^{-1}) was determined.

The quantity of Pb(II) in the wastewater sample was analyzed to be between 0.165 and 0.193 mgL^{-1}; the sample was then treated with our sorbent (SFP) to remove the Pb ions. The test revealed a not detectable (ND) limit for Pb ions (the detection limit of Pb is 0.020 mg L^{-1}). This indicates that the current sorbent is capable of removing/absorbing all Pb from the wastewater matrix.

The usual removal rate of SFP sorbent for Pb(II) was around 99.2% in DIW and subsequently declined to the minimal rates (approximately 26%, 30 mgL^{-1} Pb) in 50–100 percent seawater (Fig. 15). The findings indicated that seawater includes a high level of the major cations (Ca^{2+}, Mg^{2+} Na^{+}, and K^{+}) than DIW, tap water, and wastewater, resulting in a lower Pb(II) ions removal percent. Comparable findings on the elimination of cadmium ions by algae/chitosan composites and green algae were reported in other research [24, 66]. In addition, Nessim et al. [42] described that Pb(II) ions are often highly influenced by interfering species in seawater than in wastewater. Thus, the great concentration of cations in seawater inhibits the adsorption of Pb(II) ions.

4 Conclusions

Shells of the bivalves *Brachidontes variabilis* “*Mytilus arabicus*” collected from the northern part of the Gulf of Suez were used to create an eco-friendly shellfish powder (SFP) for the sorption of Pb ions from aquatic media. At an optimal contact period of 90 min, SFP particle size of 0.063 mm, pH 5.5, SFP dose of 0.05 g, the ambient of 25 °C, and agitation rate of 250 rpm, the maximal removal capacity of the bio-sorbent under study were attained. The experimental findings and the monolayer Langmuir sorption capacity of SFP sorbent were matched at 259.21 mgg^{-1} for Pb (II). The Pb ion dynamics on the SFP sorbent followed a quasi-1st order. Negative sign ΔG^o value indicated that Pb ion sorption by SFP sorbent occurred spontaneously. A positive sign of ΔH^o value indicates the endothermic nature of the sorption process.

Authors' contributions Safaa A. Mahmoud: planning and execution of experiments, analyses, interpretation of data, and manuscript preparation

Adel S. Orabi: supervision of the research and manuscript preparation

Lamiaa I. Mohamedein: sharing discussion and manuscript preparation

Khalid M. El-Moselhy: sharing discussion and manuscript preparation

Eman M. Saad: supervision, analysis of data, discussion, and manuscript preparation

Funding Open access funding provided by The Science, Technology & Innovation Funding Authority (STDF) in cooperation with The Egyptian Knowledge Bank (EKB). This research was funded by the Faculty of Science, Suez University; 2019-A4.

Data availability All data obtained and analyzed in this research are included as well as the supplementary data.

Declarations

Ethics approval and consent to participate Not applicable

Consent for publication Not applicable

Competing interests The authors declare no competing interests.

References

1. WHO (2021) World Health Organization Newsroom, Lead Poisoning. https://www.who.int/news-room/factsheets/detail/lead-poisoning-and-health
2. Ebrahimi SJA, Eslami A, Ebrahimzadeh L (2015) Evaluation of heavy metals concentration in the drinking water distribution network in Kurdistan Villages in the year 2012. Res. J. Pharmac. Biolog. Chem. Sci. 6(2):55–61
3. Tchounwou PB, Yedjou CG, Patlolla AK, Sutton DJ (2012) Heavy metal toxicity and the environment. Experientia supplementum 101:133–164. https://doi.org/10.1007/978-3-7643-8340-4_6
4. Barakat MA (2011) New trends in removing heavy metals from industrial wastewater. Arab. J. chem. 4(4):361–377
5. Sarvani R, Damani E, Ahmadi S (2018) Adsorption isotherm and kinetics study: removal of phenol using adsorption onto modified Pistacia mutica shells. Iran. J. Health Sci. 6:33–42
6. Alqadami AA, Naushad M, Abdalla MA, Ahmad T, Alothman ZA, Alshehri SM, Ghfar AA (2017) Efficient removal of toxic metal ions from wastewater using a recyclable nanocomposite: a study of adsorption parameters and interaction mechanism. J. Clean. Prod. 156:426–436. https://doi.org/10.1016/j.jclepro.2017.04085
7. Ashrafi M, Chamjangali M, Bagherian G, Goudarzi N, Kavian S (2017) Evaluation of nano-silica, extracted from stem sweep, as a new adsorbent for simultaneous removal of crystal violet and methylene blue from aqueous solutions. Desalin. Water Treat. 88:207–220
8. Ma W, Zong P, Cheng Z, Wang B, Sun Q (2014) Adsorption and bio-sorption of nickel ions and reuse for 2-chlorophenol catalytic ozonation oxidation degradation from water. J. Hazard. Mater. 266:19–25
9. Shojaeimehr T, Rahimpour F, Khadivi MA, Sadeghi M (2014) A modeling study by response surface methodology (RSM) and artificial neural network (ANN) on Cu2+ adsorption optimization using light expanded clay aggregate (LECA). J. Ind. Eng. Chem. 20:870–880
10. Hossain A, Bhattacharyya SR, Aditya G (2015) Biosorption of cadmium by waste shell dust of freshwater mussel Lamellidens marginalis : implications for metal bioremediation. ACS Sustainable Chem. Eng. 3(1):1–8
11. Alidoust D, Kawahigashi M, Yoshizawa S, Sumida H, Watanabe M (2015) Mechanism of cadmium biosorption from aqueous solutions using calcined oyster shells. J. Environ. Manag. 150:103–110
12. Seco-Reigosa N, Cutillas-Barreiro L, Nóvoa-Muñoz JC, Arias-Estévez M, Fernández- Sanjurjo MJ, Álvarez-Rodríguez E, Núñez-Delgado A (2014) Mixtures including wastes from the mussel shell processing industry: retention of arsenic, chromium and mercury. J. Clean. Prod. 84:680–690
13. Du Y, Zhu L, Shan G (2012) Removal of Cadmium from contaminated water by nano-sized aragonite mollusk shell and the competition of coexisting metal ions. J. Collo. Interf. Sci. 367(1):378–382
14. Lu J, Lu Z, Li X, Xu H, Li X (2015) Recycling of shell wastes into nanosized calcium carbonate powders with different phase compositions. J. Clean. Prod. 92:223–229
15. Rahman NAA, Said MIM, Azman S (2017) Carbonized green mussel shell as heavy metal removal. Malays, J. Civil Engineer., p 29
16. Terranova MS, Lo Brutto S, Arculeo M, Mitton JB (2007) Mitochondrial phylogeography of Brachidontes variabilis (Bivalvia: Mytilidae) reveals three cryptic species. J. Zoolog. Syst. emat. Evolution. Res. 45(4):289–298
17. Morton B (1988) The population dynamics and reproductive cycle of Brachidontes variabilis (Bivalvia: Mytilidae) in a Hong Kong Mangrove. Malacology. Rev. 21:109–117
18. Barash A, Danin Z (1986) Further additions to the knowledge of Indo-Pacific Mollusca in the Mediterranean Sea. Spixiana 9:117–141

19. Sasekumar A (1974) Distribution of macrofauna on a Malayan mangrove shore. J. Anim. Ecol. 43:51–69
20. Taylor JD (1971) Reef-associated molluscan assemblages in the Western Indian Ocean. Symp. Zool. Soc. Lond. 28:501–534
21. Bulut A, Yusan S, Aytas S, Sert S (2018) The use of sea shell (Donax trunculus) powder to remove Sr(II) ions from aqueous solutions. Water Sci. Technol. 78(3-4):827–836. https://doi.org/10.2166/wst.2018.353
22. Rezaei M, Pourang N, Moradi AM (2022) Removal of lead from aqueous solutions using three bio-sorbents of aquatic origin with an emphasis on the effective factors. Scient. Rep. 12:751. https://doi.org/10.1038/s41598-021-04744-0
23. Kumar AVA, Hashimi SA, Hilal N (2008) Investigation of kinetics and mechanism involved in the biosorption of heavy metals on activated sludge. Int. J. Green Energy 5:313–321
24. Saad EM, Elshaarawy RF, Mahmoud SA, El-Moselhy KM (2021) New Ulva Lactuca algae-based chitosan bio-composites for bioremediation of Cd(II) ions. J. Bioresource. & Bioprod. 6:223–242. https://doi.org/10.1016/j.jobab.2021.04.002
25. Lam YF, Lee LY, Chua SJ, Lim SS, Gan S (2016) Insights into the equilibrium, kinetic, and thermodynamics of nickel removal by environmentally friendly Lansium domesticum peel adsorbent. Ecotoxicol. Environ. Saf. 127:61–70
26. Park HJ, Jeong SW, Yang JK, Kim BG, Lee SM (2007) Removal of heavy metals using waste eggshells. J. Environ. Sci. 19(12):1436–1441
27. El-Naggar NE, Hamouda RA, Saddiq AA, Alkinani MH (2021) Simultaneous bioremediation of cationic copper ions and anionic methyl orange azo dye by brown marine alga Fucus vesiculosus. Sci. Rep 11(1):3555. https://doi.org/10.1038/s41598-021-82827-8
28. Dulla JB, Tamana MR, Boddu S, Pulipati K, Srirama K (2020) Biosorption of copper(II) onto spent biomass of Gelidiella acerosa (brown marine algae): Optimization and kinetic studies. Appl. Water Sci 10:1–0. https://doi.org/10.1007/s13201-019-1125-3
29. Xu X, Liu X, Oh M, Park J (2019) Oyster shell is a low-cost adsorbent for removing heavy metal ions from wastewater. Poll. J. Environ. Stud. 28(4):2949–2959
30. Yousefi Z, Mashayekh-Salehi A, Mohammadpour TRA (2016) Biosorption of chromium in aqueous solutions using bivalve mollusk shells through central composite design (CCD) model. Desalin. Water Treat. 57(42):19877–19889
31. Muthulakshmi Andal N, Charulatha S, Gayathri NS, Anuradha J (2016) A comparative study on the sorption of divalent ions by bivalves shells: equilibrium and statistical studies. Chem. Sci. Rev. Lett. 5(19):214–223
32. Prabu K, Shankarlal S, Natarajan E (2012) A biosorption of heavy metal ions from aqueous solutions using a fish scale (Catla catla). World J. Fish Mar. Sci. 4(1):73–77
33. Zayadi N, Othman N (2013) Characterization and optimization of heavy metals biosorption by fish scales. Adv. Mater. Res. 795:260–265
34. Villanueva-Espinosa JF, Hernández-Esparza M, Ruiz-Trevino FA (2001) Adsorptive properties of fish scales of Oreochromis niloticus (Mojarra Tilapia) for metallic ion removal from waste water. Ind. Eng. Chem. Res. 40(16):3563–3569
35. Bansal M, Mudhoo A, Garg VK, Singh D (2014) Preparation and characterization of bio sorbents and copper sequestration from simulated wastewater. Int. J. Environ. Sci. Technol. 11:1399–1412. https://doi.org/10.1007/s13762-013-0293-1
36. Hayeeye F, Yu QJ, Sattar M, Chinpa W, Sirichote O (2018) Adsorption of Pb^{2+} ions from aqueous solutions by gelatin/activated carbon composite bead form. Adsorb. Sci. Technol. 36(1–2):355–371
37. Aly HM, Shama SA, Elsharkawy AM, Helal AI, Khodir AM (2016) Adsorption of Cu^{2+} ion from aqueous solution by clamshell powder. Benha J. Applied Sci. (BJAS) 1(1):43–51
38. Abdel-Ghani NT, El-Chaghaby GA (2014) Biosorption for metal ions removal from aqueous solutions: a review of recent studies. Int. J. Lat. Res. Sci. Technol. 3(1):24–42
39. Akpomie KG, Dawodu FA, Adebowale KO (2015) The mechanism of the sorption of heavy metals from binary solution by low-cost montmorillonite and its desorption potential. Alex. Engineer. J. 54:757–767. https://doi.org/10.1016/j.aej.2015.03.025
40. Barka N, Abdennouri M, Makhfouk ME, Qourzal S (2013) Biosorption characteristics of cadmium, lead to eco-friendly dried cactus cladodes. J. Environ. Chem. Eng. 1(3):144–149. https://doi.org/10.1016/j.jece.2013.04.008
41. Karthikeyan G, Anbalagan K, Muthulakshimi AN (2004) Adsorption dynamics and equilibrium studies of Zn(II) onto chitosan. J. Chem. Sci. 116:119–127
42. Nessim RB, Bassiouny AR, Zaki HR, Moawad MN, Kandeel KM (2011) Biosorption of lead and cadmium using marine algae. Chem. Ecol. 27:579–594
43. Yang L (2007) Biosorption of copper and chromium by Sargassum sp. determination of biosorption properties and investigation of metal-sorbent interactions. The National University of Singapore
44. Al-Qodah Z (2006) Biosorption of heavy metal ions from aqueous solutions by activated sludge. Desalination 196:164–176. https://doi.org/10.1016/j.desal.2005.12.012
45. Putra WP, Kamari A, Yusoff SNM, Ishak CF, Mohamed A, Hashim N, Isa IM (2014) Biosorption of Cu(II), Pb(II), and Zn(II) ions from aqueous solutions using selected waste materials: adsorption and characterization studies. J. Enca. & Ads. Sci. 4:25–35
46. Kumar D, Gaur JP (2011) Metal biosorption by two cyanobacterial mats about pH, biomass concentration, pretreatment, and reuse. Bioresour. Technol. 102:2529–2535
47. Rathinam A, Maharshi B, Janardhanan SK, Jonnalagadda RR, Nair BU (2010) Biosorption of cadmium metal ion from simulated wastewaters using Hypnea valentiae biomass: a kinetic and thermodynamic study. Bioresour. Technol. 101:1466–1470
48. Mall DI, Srivastava VC, Agarwal NK (2006) Removal of Orange-G and methyl violet dyes by adsorption onto bagasse fly ash kinetic study and equilibrium isotherm analyses. Dye. Pigment. 69:210–223
49. Senthil KP, Ramalingam S, Sathyaselvabala S, Kirupha SD, Sivanesan S (2010) Removal of copper (II) ions from aqueous solution by adsorption using cashew nut shell. Desalination 266:1–31
50. Sofiane B, Sofia KS (2015) Biosorption of heavy metals by chitin and chitosan. Der Pharma Chem. 7:54–63
51. Kyzas ZG (2012) Commercial coffee wastes as materials for adsorption of heavy metals from aqueous solutions. Materials 5:1826–1840. https://doi.org/10.3390/ma5101826
52. Elsayed SA, Saad EM, Butler IS, Mostafa SI (2018) 2-Hydroxynaphthaldehyde chitosan Schiff-base; new complexes, bio sorbent to remove cadmium(II) ions from aqueous media and aquatic ecotoxicity against green alga Pseudokirchneriella subcapitata. J. Environ. Chem. Eng. 6(2):3451–3468. https://doi.org/10.1016/j.jece.2017.12.051
53. Mostafa SI, Ali MA, El-Wassefy NA, Saad EM, Hussein MH (2022) Adsorption and interaction studies of methylene blue dye onto agar-carboxymethylcellulose-silver nanocomposite in aqueous media. Biomass Conversion and Biorefinery 21:1–21. https://doi.org/10.1007/s13399-022-02505-1
54. Zheng H, Wang Y, Zheng Y, Zhang HM, Liang SP, Long M (2008) Equilibrium, kinetic and thermodynamic studies on the sorption of 4-hydroxyphenyl on Cr-bentonite. Chem. Eng. J. 143:117–123
55. Goldberg S (2018) Equations and models describing adsorption processes in soils. SSSA Book Series. Madison, WI, USA: Soil Science Society of America 2018:489–517

56. Saad EM, Hassan HM, Soltan MS, Butler IS, Mostafa SI (2018) Removal of copper(II) ions from aqueous media by chemically modified MCM-41 with N-(3- (trimethoxysilyl)propyl)ethylenediamine and its 4-hydroxysalicylidene schiff-base. Environ. Prog. Sus. Ener. 37:746–760
57. Dubinin MM, Zaverina ED, Radushkevich LV (1947) Sorption and structure of active carbons. I. Adsorption of organic vapors. Zh. Fiz. Khim. 21:1351–1362
58. El-Nemr MA, Yilmaz M, Ragab S, El Nemr A (2022) Biochar-SO prepared from pea peels by dehydration with sulfuric acid improves the adsorption of Crz^{6+} from water. Bioref, Biomass Conv. https://doi.org/10.1007/s13399-022-02378-4
59. Temkin MI, Pyzhev VM (1940) Kinetics of ammonia synthesis on promoted iron catalysts. Acta Physicochim. 12:327–352
60. Zheng H, Liu DH, Zheng Y, Liang SP, Liu Z (2009) Sorption isotherm and kinetic modeling of aniline on Cr-bentonite. J. Hazard. Mater. 167:141–147
61. Lagergren S (1907) Zur Theorie der sogenannten Adsorption gelöster Stoffe. Zeitschrift Für Chemie Und Ind. Der Kolloide 2:15
62. Ho YS, McKay G (1999) Pseudo-second order model for sorption processes. Process. Biochem. 34:451–465
63. Li ZC, Fan HT, Zhang Y, Chen MX, Yu ZY, Cao XQ, Sun T (2011) Cd(II)-imprinted polymer sorbents prepared by combination of surface imprinting technique with hydrothermal assisted Sol-gel process for selective removal of cadmium(II) from aqueous solution. Chem. Eng. J. 171:703–710
64. Nuhoglu Y, Malkoc E (2009) Thermodynamics and kinetic studies for environmentally friendly Ni(II) biosorption using waste pomace of olive oil factory. Bioresour. Technol. 100:2375–2380
65. Wang T, Jiao Y, He M, Ouyang W, Lin C, Liu X (2022) Facile co-removal of As(V) and Sb(V) from aqueous solution using Fe-Cu binary oxides: Structural modification and self-driven force field of copper oxides. Sci. Tot. Environ. 803:150084
66. Ghoneim MM, El-Desoky HS, El-Moselhy KM, Amer A, Abou El-Naga EH, Mohamedein LI, Al-Prol AE (2014) Removal of cadmium from aqueous solution using marine green algae, Ulva lactuca. Egypt. J. Aquat. Res. 40:235–242